ORNL/TM-7898
Dist. Category UC-20 a,b,g

Contract No. W-7405-eng-26

ORNL/TM--7898

DE83 006363

FUSION ENERGY DIVISION

CONSTRAINED RIPPLE OPTIMIZATION OF TOKAMAK BUNDLE DIVERTORS

L. M. Hively
General Electric Company
Fusion Engineering Design Center

J. A. Rome
V. E. Lynch
J. F. Lyon
R. H. Fowler
Y-K. M. Peng
R. A. Dory
Fusion Energy Division

NOTICE This document contains information of a preliminary nature. It is subject to revision or correction and therefore does not represent a final report.

Date Published - February 1983

Prepared by the
OAK RIDGE NATIONAL LABORATORY
Oak Ridge, Tennessee 37830
operated by
UNION CARBIDE CORPORATION
for the
DEPARTMENT OF ENERGY

CONTENTS

ABSTRACT v

I. INTRODUCTION 1

II. DELETERIOUS PHYSICS EFFECTS 3

II.A Effects on the Plasma Equilibrium 4

II.B Fast Ion Effects 5

II.C Comparison with Other Calculations and Experiment .. 12

III. CONSIDERATIONS IN BUNDLE DIVERTOR DESIGN 13

III.A General Considerations 14

III.B Considerations for ISX-B 15

III.C Considerations for Tokamak Reactors 17

IV. DIVERTOR OPTIMIZATION 18

IV.A Assumptions for Optimization 19

IV.B Examples 20

IV.C Discussion 24

V. CONCLUSIONS AND SUMMARY 26

ACKNOWLEDGMENTS 28

APPENDIX: DIVERTOR OPTIMIZATION TECHNIQUE 29

REFERENCES 34

ABSTRACT

Magnetic field ripple from a tokamak bundle divertor is localized to a small toroidal sector and must be treated differently from the usual (distributed) toroidal field (TF) coil ripple. Generally, in a tokamak with an unoptimized divertor design, all of the banana-trapped fast ions are quickly lost due to banana drift diffusion or to trapping between the 1/R variation in $|\vec{B}| \equiv B$ and local field maxima due to the divertor.

Studying the full three-dimensional shape of the B-surfaces allows quick evaluation of many inferior designs. For designs that eliminate any large maxima in B, low on-axis ripple is a good indicator of avoiding deleterious effects due to the divertor. However, this must be achieved while satisfying many engineering constraints.

A computer code has been written to optimize automatically on-axis ripple subject to these constraints, while varying up to nine design parameters. Optimum configurations have low on-axis ripple (<0.2%) so that, now, most banana-trapped fast ions are confined. Only those ions with banana tips near the outside region ($|\theta| \leq 45^{o}$) are lost. However, because finite-sized TF coils have not been used in this study, the flux bundle is not expanded.

1. INTRODUCTION

Fusion reactor operation may require active control of impurities as well as control of particle and heat fluxes to the wall. One means of such control on a tokamak may be through the use of a bundle divertor.[1-2] A set of external field coils opposing the main toroidal field forms the basic divertor magnetic geometry: a separatrix in the field line topology[1] (due to two null points in $|\vec{B}|$) and a line null in the toroidal field (TF), B_ϕ. The separatrix passes from the plasma edge, through the line of $B_\phi = 0$, and into the divertor; this is the first diverted field line. Divertor control is then a result of charged particles following the diverted magnetic field lines out of the tokamak, through the divertor throat, and into a collector/pumping region. Another type of magnetic divertor is the more familiar poloidal divertor,[3-4] which produces one or more line nulls in the poloidal, rather than the toroidal, field. Bundle divertors may be easier to implement than poloidal divertors because they are compact and do not link the TF coils. However, the TF null in a bundle divertor creates a large, localized magnetic perturbation. As a result, there may be an unacceptable loss of fast ions or large perturbations in the poloidal flux surfaces with an attendant enhancement of plasma transport or disruptions. Whereas past work on bundle divertors has emphasized engineering optimization,[5] here we include the additional physics effects of the magnetic ripple as well.

Since the bundle divertor was first suggested in 1972 by Colven et al.,[6] extensive work has been done. The simple two-coil bundle divertor has been carefully studied (e.g., see Refs 1, 2, and 6 through 9); however, the resulting on-axis ripple is large and may significantly degrade confinement of fast ions in a reactor. Two-coil configurations with flux bundle expander coils have been investigated (e.g., see Refs 7 and 10 and citations therein), but the ripple may also be too large for reactor application. References 11 and 12 have pursued four-coil divertors with a large magnetic octopole component and small dipole and quadrupole moments to produce low ripple. However, because of the higher order field, those designs require large coil currents with correspondingly large power dissipation, high current density, and strong forces and torques, thus making engineering implementation difficult. These four-coil divertors also make expansion of the diverted flux bundle difficult because the field lines lie close to the central legs of the divertor. Another unfortunate result is the high mirror ratio, which causes reflection of many diverted ions. These reflected ions may hit the divertor structure and cause surface damage and impurity evolution. Thus, the design of bundle divertors is complicated by the conflicting requirements of physics and engineering. For example, a divertor has been constructed for the Impurity Studies Experiment (ISX-B) (Ref. 8) that has improvements beyond the basic configuration.[1] However, this divertor will produce an on-axis ripple of 1.6%, which is predicted to be excessive for reactor application. In light of the above experience, it is necessary to examine both the engineering and the physics constraints in order to obtain a better divertor design.

The present work endeavors to minimize ripple effects while satisfying reactor-relevant engineering constraints. In Sec. II, the effects of local ripple on the plasma are described, including fast ion confinement and ripple-induced ergodicity of the equilibrium. Section III considers criteria for divertor design in the light of the previous section. The assumptions and techniques for divertor optimization are presented in Sec. IV and several example calculations are given for ISX-B and the Engineering Test Facility/International Tokamak Reactor (ETF/INTOR). Finally, Sec. V discusses our results and conclusions.

II. DELETERIOUS PHYSICS EFFECTS

Deleterious effects on fast ion and plasma confinement may result from bundle divertor ripple and the concomitant breaking of axisymmetry. The effects of most importance are perturbations in the plasma equilibrium and loss of collisionless energetic ions. The ripple enhancement of the ion heat conductivity and diffusion coefficients has been discussed elsewhere (e.g., see Refs 13 through 17) and is not repeated here.

II.A Effects on the Plasma Equilibrium

The magnetic properties of a divertor are partially determined by the poloidal flux surface topology in the plasma. A badly designed divertor may ergodize the field lines and degrade containment of the background plasma. This effect is highly model dependent and is very sensitive to the q profile of the plasma. Low order rational surfaces near the plasma edge can interact strongly with the low harmonic part of the local ripple fields, causing the field lines at the edge of the plasma to become ergodic.[18] To determine the consequences of the ripple, one should model the complete three-dimensional magnetic field of the tokamak. However, present three-dimensional equilibrium codes have insufficient resolution to properly handle islands and ergodic regions in a tokamak geometry. We have therefore adopted the following expedient model: the magnetic field is the sum of an axisymmetric two-dimensional (noncircular) equilibrium field and the vacuum divertor field, which is calculated using the Biot-Savart law assuming filamentary coils. This model predicts a bulge in the flux surfaces near the divertor as well as islands and ergodic regions. These perturbations arise from reconnecting field lines across the divertor region; fields and currents far from the divertor are unperturbed.

The divertor creates a minimum in $|\vec{B}| \equiv B$, causing the plasma to bulge outward toward the divertor. Also, the ripple may interact with the rational surfaces in the plasma and with any tearing modes that may be present to produce islands and/or ergodic regions. To calculate these perturbations, various field lines are followed 300 to 500 times around the torus to map out the poloidal flux surfaces. Although the

poloidal flux surface far from the divertor may be drastically altered, the magnitude of the field is essentially unchanged in this region. For example, Fig. 1 shows the flux surfaces calculated for ETF/INTOR with a four-coil bundle divertor; the same equilibrium was used in each case, but the equilibrium was scaled to give different values of q_{edge}. Because the $q = 2$ surface interacts strongly with the ripple, flux surfaces with $q_{edge} \simeq 2$ are much worse than those with $q_{edge} \simeq 4$. Thus, tokamaks with bundle divertors may need to operate at a very low (≤ 2) or high (≥ 3) value of q_{edge}. Multiple bundle divertors can reduce flux surface perturbations by lowering the toroidal harmonic ripple content but at the price of increasing the probability of fast ion loss.

II.B Fast Ion Effects

There has been considerable work on ripple-induced fast ion transport including analytical as well as computer code calculations (e.g., see Refs 13 through 17 and 19 through 21). All of these studies, excluding Ref. 19, considered periodic ripple effects due to the discrete TF coils in tokamaks. Vertically asymmetric ripple-assisted injection was examined in Ref. 19. Fast ion orbits in diverted tokamaks can be analyzed by field-line-orbit codes (e.g., Ref. 17) using numerical integration of the collisionless guiding center equations. A full evaluation requires the inclusion of collisional effects and is presently under study.[22]

Magnetic ripple in tokamaks destroys axisymmetry and thereby eliminates the toroidal canonical angular momentum P_ϕ as an exact constant of the motion. In one resulting process, an ion can be collisionlessly trapped due to its finite orbit size where there is insufficient parallel velocity $v_\parallel$ to escape from a ripple well; this is termed ripple trapping.[15] As the ion oscillates within the well, it drifts vertically into larger ripple and is lost. Another process is collisional ripple trapping due to pitch-angle scattering as a large banana-width orbit traverses a B-field minimum with $v_\parallel/v \simeq 0$. Collisional detrapping occurs by the inverse process. There is also banana-drift diffusion[13] because the large banana-width orbits fail to close exactly. This arises from a ripple-induced "variable lingering period" as the $v_\parallel/v \simeq 0$ part of an orbit passes through a magnetic well. All these mechanisms can cause radial transport and loss of superthermal ions, thus degrading plasma heating by neutral beams and fusion products.

The magnetic well created by a bundle divertor is localized on the outboard edge of the tokamak near the equatorial plane, so (barely trapped) particles with $v_\parallel \simeq 0$ on the midplane are affected the most. When 3.5-MeV alpha particles are born and trapped in this well, they are rapidly lost. However, the effect of this loss is small because the low plasma edge density and temperature yield a low alpha source rate. A similar loss of neutral beam ions can be avoided by tilting the injectors away from the perpendicular direction ($>15^\circ$). Our numerical studies have only rarely encountered collisionless trapping because competing loss processes are more rapid and because toroidal drift of the banana orbits may make the wells inaccessible.[20] While

collisional ripple trapping rates can be significant,[20] this paper concentrates on more important collisionless processes for fast ions in bundle divertor ripple.

Usually, the bundle divertor field produces a local maximum in B on each side of the ripple well, yielding a new ripple-produced trapping process. In particular, a banana-trapped particle can become ripple-trapped between the divertor-created maximum and the usual 1/R increase in the TF and then rapidly drift out of the tokamak. Figure 2 shows an example of such a particle guiding center orbit for a double-T bundle divertor design on ETF/INTOR due to Yang.[11]

Outward drift due to ripple can still be present even if a banana-trapped ion is not lost by the above process. Figure 3 shows such an orbit in ETF/INTOR as it drifts to the wall. (Collisions among lower energy ions can convert this to diffusion, but this drift is the dominant loss process for fast ions.) It is easy to estimate the magnitude of the radial step size for each orbit in the following manner. In an axisymmetric tokamak, P_ϕ is given by

$$P_\phi = mv_\parallel \frac{F}{B} - e\psi \ , \tag{1}$$

where

$$v_\parallel = \pm\left[\frac{2}{m}\left(\varepsilon - \mu B\right)\right]^{1/2} \ , \tag{2}$$

$F(\psi) \equiv RB_{toroidal}$, m and e = mass and charge of the fast ion, and ψ = the poloidal flux function. The particle energy is ε, with magnetic

moment $\mu = 1/2\ mv_{\perp}^2$. Equations (1) and (2) may be solved for B as a function of ψ and expanded near the banana tip to yield

$$B(\psi) \simeq \frac{\varepsilon}{\mu} - \frac{m\varepsilon^2}{2\mu^3}\left[\frac{e}{mF}\ (\psi - \psi_{tip})\right]^2 . \tag{3}$$

This last expression can be expanded to give

$$B(\psi) \simeq B_{tip}\left[1 - \left(\frac{\omega_{c_{tip}}}{vF_{tip}}\right)^2 (\psi - \psi_{tip})^2\right], \tag{4}$$

where "tip" indicates evaluation at the banana tip location in the absence of the ripple and ω_c is the ion cyclotron frequency. The localized ripple is modeled by a jump ΔB in B near the divertor. The ion then mirrors at the point along its orbit (subscript M) where

$$B(\psi_M) = B_{tip} - \Delta B = B_{tip}\left[1 - \left(\frac{\omega_{c_{tip}}}{vF_{tip}}\right)^2 (\psi_M - \psi_{tip})^2\right], \tag{5}$$

and hence

$$\psi_M = \psi_{tip} + \left(\frac{\Delta B}{B_{tip}}\right)^{1/2}\left(\frac{vF_{tip}}{\omega_{c_{tip}}}\right). \tag{6}$$

On reaching this point, the particle reverses direction, leaving with the same speed as it entered. After the bounce, the new value of P_ϕ will be

$$P_\phi = -mv_\parallel \frac{F_M}{B_M} - e\psi_M \simeq -e\psi_{tip} - 2e\left(\frac{\Delta B}{B_{tip}}\right)^{1/2}\left(\frac{vF_{tip}}{\omega_{c_{tip}}}\right), \tag{7}$$

where the factor of 2 arises from both the co- and countergoing portions of the banana orbit encountering the ripple well. Since this is just $e\psi$ at the new banana tip location, the change in ψ at the banana tip is given by

$$\Delta\psi \simeq 2\left(\frac{\Delta B}{B}\right)^{1/2}\left(\frac{vF_{tip}}{\omega_{c_{tip}}}\right). \tag{8}$$

Actually, $\Delta\psi$ corresponds to the maximum radial excursion because the model ripple will also reflect any ion with $B_{tip} - B_M < \Delta B$. This radial excursion will be outward for an ion approaching the tip on the outer half of a banana and inward for an ion on the inner portion. Since the ripple is stronger on the outboard side of the tokamak, the outward steps will be larger than the inward steps, and thus outward drift occurs. Note also that an abrupt minimum in B will cause a banana orbit to continue past its unperturbed tip location, and the reverse of the above processes may occur.

Although P_ϕ is no longer a constant of the motion, it should be constant in regions where nonaxisymmetric fields have decayed to negligible values. Thus, P_ϕ is constant when the particle is far from the ripple and may change abruptly as it passes near the divertor. Often, a surprising feature of P_ϕ versus time is its quasi-periodicity for circulating particles and its lack of periodicity for bananas.[23] Figures 4 and 5 show two such cases for ETF with a double-T divertor.

The random nature of P_ϕ for the banana is indicative of ripple drift to the wall. The periodicity of P_ϕ for the circulating ion indicates that a new invariant exists and that the ion is collisionlessly well confined. Since the P_ϕ is actually quasi-periodic, another test is necessary to ensure that a new invariant of the motion really exists.

This is done by plotting where the guiding-center orbit intersects a plane, at a fixed toroidal angle, in the course of 50-100 revolutions around the tokamak. Figure 5(c) shows the resulting puncture plot, demonstrating well-formed (nonergodic) islands. The periodic nature of P_ϕ correlates well with the existence of a nonergodic puncture plot and takes much less time to compute than following 10^3 toroidal transits to determine confinement or loss.

The existence of a new invariant does not mean that the invariant is easy to find or that it is useful in determining the orbit. This is apparently the case for tokamaks with local field ripple. For example, the invariant might be defined as the area under one quasi-period of the P_ϕ plot. This invariant applies on time scales much longer than a bounce time and thus is less useful than P_ϕ, which is valid instantaneously. A more fruitful approach might be to regard the effect of the divertor region as a mapping since the orbit has three good constants of motion away from the divertor region and P_ϕ changes only when passing near the divertor. However, for realistic divertor fields, it appears that this mapping can only be studied numerically.

Since the maxima and minima in B lead to ripple trapping and radial motion of banana-trapped ions, studying the shape of constant B surfaces can provide a fast, efficient indication of energetic ion confinement. This technique is inherently global and does not require solving differential equations. At low beta, in the absence of the divertor, these surfaces are cylinders, since $B \sim 1/R$.

In an axisymmetric high beta equilibrium, the plasma digs its own well, and hence there is a minimum in B on the outboard side of the magnetic axis. With this high beta equilibrium topology in mind, Fig. 6 shows the B = constant surfaces for a simple two-coil divertor in ETF/INTOR. The closed B surfaces away from the divertor are a result of the axisymmetric, high beta, minimum-B well discussed above. On each side of the divertor there is a maximum in B, causing some of the B surfaces to become closed. Banana orbits whose mirror points occur on these surfaces cannot get past the toroidal maxima and are poorly confined. Similar effects arise from surfaces that shrink significantly upon reaching the divertor region. Thus, without following any field lines or orbits, this divertor design is quickly seen to be poor. In contrast, Fig. 7 shows a four-coil divertor that has been configured to eliminate the maxima in B. There is only very slight narrowing of the B-surface cross section and a better divertor design results.

II.C Comparison with Other Calculations and Experiment

The consequences of field line ergodicity and fast-ion loss form a basis for minimizing the magnetic ripple due to a bundle divertor. It is therefore appropriate to compare our results with other calculations and with existing experimental data. We note, however, that present calculations do not use self-consistent models, and there have not yet been any bundle divertor experiments that can be extrapolated to ETF/INTOR conditions.

Although flux surface perturbations appear important, the evidence for this effect is not currently clear. Localized ripple effects have been modeled for the Princeton Large Tokamak (PLT) with a partially shorted TF coil[24] and for ST (Ref. 25). These calculations showed an absence of islands when a simple poloidal field (PF) pattern was displaced radially by different amounts around the torus to simulate current flow along a perturbed magnetic axis. Calculations by Stott et al.[1] for the DITE bundle divertor also showed an absence of islands with a scale size >1 mm. On the other hand, Bateman and Morris[26] have done a more self-consistent calculation showing that the size of magnetohydrodynamic mode islands may be either raised or lowered by a bundle divertor.

Bundle divertor studies[27] in the Divertor and Injection Tokamak Experiment (DITE) at relatively low density and temperature do not show the enhanced transport that would accompany large islands or ergodic regions. Experiments[28] on ISX-B have included a set of eyeglass-shaped ripple coils that can produce the same on-axis field perturbation as the ISX-B bundle divertor but with a smaller edge ripple and a

different radial gradient. There is very little effect on the plasma transport or stability below a certain ripple level. Above this threshold, the plasma disrupts. Further bundle divertor experiments at high densities and temperatures are needed to clarify this issue.

Currently there is no strong evidence for significant fast ion loss due to localized ripple. This null result has been obtained in preliminary DITE bundle divertor experiments with injection at low plasma currents.[27] The ISX-B experiments[28] with the "eyeglass" ripple coils also show no significant loss of high energy ions nor any change in the resulting ion temperature. However, such losses are seen on ISX-B when neutral beam ions are injected directly into the ripple well. A firm conclusion about local-ripple-induced energetic ion losses awaits improvements in the experiments.

Since the effect of localized field ripple on the plasma behavior is still not certain, it is prudent to assume that such effects are important. Consequently, minimizing these effects leads to a conservative set of bundle divertor optimization criteria.

III. CONSIDERATIONS IN BUNDLE DIVERTOR DESIGN

There are several important physics and engineering problems that have a strong impact on divertor design in both general and device-specific ways.

III.A General Considerations

Divertor operation requires that the plasma be connected to the divertor separatrix by a field line. This line must continue through the divertor without intersecting any structure; the same constraint applies to field lines outside the separatrix (the scrapeoff region) that go through the divertor. Thus, the bore of each coil must allow for the diverted flux bundle, as well as for the support structure, neutron shielding, electrical insulation, and finite coil cross section. Expansion of the diverted flux bundle is desirable (and perhaps necessary) to spread the plasma heat load over a sufficient collector area (20 m^2 to handle 100 MW in ETF). Without expansion, the heat flux could be distributed among several divertors, but the capital cost would then become prohibitive. Normal copper coils were selected for ETF due to space constraints and neutron damage considerations;* hence, the resulting power dissipation must be kept to a credible level.

The average current density in the coils is limited by the coolant flow through the hollow copper conductor. The space constraints in the divertor throat require higher current, larger size divertor coils that are farther from the plasma edge; reducing power dissipation, current density, and ripple effects requires lower current, smaller size divertor coils close to the plasma edge. For good plasma confinement, it may be necessary to reduce the ripple over the whole plasma cross

*The use of superconducting coils requires at least 0.25 m of shielding in FED (0.5 m in ETF) and a lower coil current density than used for copper coils. The resulting divertor creates unacceptably high ripple.

section (not just in the midplane). However, the ripple δ at the separatrix is unavoidably large (~90%) due to the null in B_ϕ (the PF is still nonzero), where $\delta = (B_{max} - B_{min})/(B_{max} + B_{min})$ along a given field line. Satisfying these conflicting criteria is a difficult task, as discussed in detail below.

III.B Considerations for ISX-B

To evaluate how well the ISX-B divertor satisfies these criteria, we next examine the two-solenoid ISX-B divertor,[8] designed by T. Yang of the Massachusetts Institute of Technology (MIT). The resulting surfaces of constant B are also shown for a low beta, ISX-B equilibrium (see Fig. 8); the maxima pull the otherwise cylindrical B surfaces against the outside wall, thus blocking some bananas. Figure 9 shows contours of constant ripple in the poloidal plane without plasma current; on-axis ripple is 1.6% and rises steeply toward the divertor. Figure 10 shows a map of the field lines from the plasma to the divertor plate. Plasma motion along these diverted field lines can then be used to determine the heat loading on the divertor collection plate; the plate design can then be modified to give a more uniform heating.

The low plasma current in ISX-B (<220 kA) may result in poor fast ion confinement because ions on large banana-width orbits can reach the wall in less than one bounce period (<30 μs). Since ISX-B uses a high power, 35- to 40-keV H^0 beam, it is necessary to assess these losses in the presence of ripple. Figure 11 summarizes the confinement of collisionless 40-keV protons in the constants-of-motion space of Ref. 29. In this space, orbits are labeled by v, the ion speed; ψ_x, the maximum value of the poloidal flux function ψ along the guiding-center orbit, where ψ is increasing from the magnetic axis; and ζ, the cosine of the angle between the parallel component of plasma current and the ion velocity at ψ_x, that is, $\zeta = [\vec{J}_\parallel \cdot \vec{v}/(|\vec{J}_\parallel| \cdot v)|_{\psi_x}]$. Trapped particles are represented only once in this space for $\zeta > 0$ because $\vec{J}_\parallel \cdot \vec{v}$ is always positive on the outboard part of the banana. The region near $\zeta = 0$ and $\psi_x = 0$ is forbidden in order to maintain the single-valuedness of the space. Numerous orbits were followed until they hit the wall or until the puncture plot was well defined. As expected, the banana-trapped ions are lost due to ripple effects. Ions near the outside of the plasma and with $\zeta \sim 1$ are properly diverted. However, circulating ions near the plasma edge with a pitch angle $\zeta < 0.8$ are reflected by the large mirror ratio (~3.5) in the divertor, either hitting the divertor coils or returning to the plasma. Co- and countercirculating ions are generally well confined except for those near the plasma edge. The loss of countergoing ions near the edge is somewhat surprising since they extend beyond the separatrix only at the inboard edge where the ripple is low. However, as discussed in Sec. II.A, ripple-induced ergodicity in the outer flux surfaces can enhance edge losses. The

fast ion birth distribution for tangential injection in ISX-B has been determined by the NFREYA Monte Carlo beam deposition code[30] and is plotted in Fig. 12. The fast ion birth points in ψ_x, ζ space lie to the right of the banana-trapping region ($\zeta > \zeta_{trapped}$), corresponding to mostly well-contained circulating particles. During thermalization, about half of these ions pitch angle scatter toward the banana-trapping (loss) boundary. However, most beam ions deposit their energy in the plasma before being lost, since the large majority are born near the plasma center.

III.C Considerations for Tokamak Reactors

Since physics and engineering problems must be solved simultaneously, a satisfactory divertor cannot be designed for ETF/INTOR as an afterthought. Rather, the reactor parameters must be guided, in part, by the divertor requirements. A key issue is the value of the TF at the plasma edge that the divertor must cancel to form a separatrix. In sharp contrast to the present, low field, diverted tokamaks with $B_\phi \leq 1.5$ T, this field will be 4 to 5 T in ETF/INTOR. In addition, the divertor field adds to the TF on the outboard side of the divertor, causing contraction of the flux bundle unless the outer legs of the TF coils lie inside the major radius of the bundle expansion zone. Also, the divertor current increases in proportion to the value of B_ϕ which must be nulled, leading to larger cross-section copper coils to meet the power dissipation and maximum current density limits. As the coil size grows, the front set of coils

must be placed further from the plasma, since the divertor must lie outside the scrapeoff zone. Consequently, more current is needed to null the TF, making it even more difficult to satisfy the design constraints. Finally, we note that a reactor is more sensitive to ripple than present tokamaks. This is because multimillion electron volt fusion products are very collisionless and therefore must be confined for several tenths of a second until their energy is transferred to the plasma. As we demonstrate in Sec. V, reduction of these difficulties points toward a larger minor radius, smaller major radius, lower-B field configuration for a tokamak reactor with a bundle divertor.

IV. DIVERTOR OPTIMIZATION

Whereas the physics and engineering concerns, as discussed above, are important, they cannot yet be modeled in detail. It is therefore necessary to make simplifying assumptions to obtain an optimized divertor configuration.

IV.A Assumptions for Optimization

Implementing a bundle divertor on ETF requires minimizing fast ion losses due to localized $\vec{B}$ field ripple, while satisfying appropriate engineering constraints. Although fast ion confinement is dependent on the detailed tokamak field topology, our studies show that minimizing ripple at the magnetic axis of the plasma also minimizes off-axis ripple (see Fig. 9). Consequently, our work has endeavored to minimize on-axis ripple, hereafter referred to simply as "ripple." The present design criterion for ETF/INTOR is $\delta < 0.3\%$ since our studies show that collisionless fast ion losses become intolerable if $\delta > 0.3\%$. The values of B_{min} and B_{max} are obtained by first picking a point on axis and toroidally far from the divertor, then moving along that $\vec{B}$-line toward the divertor assuming no plasma current. This is done[17] by integrating the coupled set of ordinary differential equations described by

$$d\vec{x}/ds = \vec{B}/|\vec{B}| \ , \qquad (9)$$

where s is the path length along the field line. Each leg of the divertor is modeled by a single filament; TF ripple is not currently included.

The engineering assumptions for the divertor optimization are shown in Table I. The value of $S_b < S_f$ has been used because the neutron reflection coefficient inside the divertor is probably <0.6 although a three-dimensional shielding calculation is ultimately needed. Structural considerations have not been included in this analysis. Instead, we simply assume that the support structure is positioned outside the active divertor region so as not to interfere with the divertor action or with shielding restrictions. Previous work has failed to find an acceptable four-coil design from an engineering viewpoint, so present studies have concentrated on the double-T coil divertor (see Figs 4, 5, and 13) first proposed by T. Yang of MIT (Ref. 11). See the Appendix for details of the optimization technique.

IV.B Examples

The double-T coil divertor has been optimized for ISX-B since the present (unoptimized) design is predicted to have large ripple effects. The assumptions for the calculation are listed in Table I, with the optimized divertor parameters given in Table II. Although the present model is capable of including discrete TF coil effects, computing time limitations do not permit this. Thus, the optimized configuration was analyzed by a field-line-plotting code[31] and found to have an unexpanded flux bundle with a ripple of 0.21% (including TF ripple). Although additional expander coils would have to be added to make this design practical, this represents almost an eight-fold ripple reduction in comparison with the two-coil divertor discussed in Sec. III.B.

TABLE I. ENGINEERING ASSUMPTIONS FOR DIVERTOR DESIGN[a]

Symbol	Description	ETF	ISX-B
S_f (m)	Nuclear shielding thickness (front)	0.3	0.0
S_b (m)	Nuclear shielding thickness (back)	0.2	0.0
f_{pk}	Electrical conductor packing fraction	0.62	0.62
ρ (Ω•m)	Resistivity of copper (160°C)	2.9×10^{-8}	2.9×10^{-8}
T_{so} (m)	Thickness of plasma scrape-off region	0.20	0.07
X_h (m)	Hole width through divertor coils	0.3	0.1
Y_h (m)	Hole height through divertor coils	0.4	0.1
P (MW)	Resistive power dissipation	100	4
J (MA/m^2)	Current density in copper coils	60[b]	60

[a]See Fig. 13.

[b]Based on normal-conducting magnet design of R. A. DANDL, H. O. EASON, A. C. ENGLAND, G. E. GUEST, C. L. HEDRICK, et al., Oak Ridge National Laboratory Rep. ORNL/TM-3684 (November 1971), p. 67, assuming $f_{pk} = 1$.

TABLE II. OPTIMIZED DIVERTOR PARAMETERS

Parameter	ISX-B	ETF[a,b]		FED[a,c]	
		Shielded	Unshielded	Shielded	Unshielded
R_o (m)	0.935	5.500		5.000	
R_{edge} (m)	1.18	6.72		6.08	
B_o (T)	1.80	5.50		3.62	
δ (%)	0.34[d]	1.83	0.27	0.87	0.08[d]

[a]The sequel to ETF has been designated FED. The device parameters given here should be taken as representative of the generic FED/ETF design.

[b]"ETF Interim Design Description Document," ETF Design Center, Oak Ridge National Laboratory (July 1980).

[c]C. A. FLANAGAN, D. STEINER, and G. E. SMITH, Fusion Engineering Design Center Staff, Oak Ridge National Laboratory Rep. ORNL/TM-7777 (June 1981).

[d]See Table A.1 for details of these cases.

Optimization of a nuclear-shielded double-T divertor (see Fig. 13) for FED has yielded an unacceptably high ripple (see Fig. 14); a shielded double-T divertor for ETF/INTOR also produces an unsatisfactory ripple. This is because a large copper coil cross section is required to meet the power dissipation and current density restrictions. This large coil cross section (plus the shielding thickness) forces the divertor to be "far" from the plasma edge so that the magnetic scrape-off zone does not intersect the divertor structure. Consequently, large coil currents are required to form the separatrix, yielding ripple values that are too high.

Optimization of an unshielded, double-T divertor on FED (and ETF/INTOR) results in acceptable ripple (see Fig. 14) with a small T-coil close to the plasma and a larger, almost planar, back T-coil. Without shielding, the divertor can be placed "close" to the plasma, dramatically lowering both the coil currents and the resulting ripple. Note that designing a bundle divertor for ETF/INTOR is especially difficult because there is a large TF to null (5.5 T). The FED case is easier due to the lower field (3.6 T). However, an unshielded divertor on ETF/INTOR (an ignited device) may not be feasible since the high neutron fluence would cause electrical insulation failure after about one year. On the other hand, an unshielded divertor on FED (a subignition device) would have a ten-year life, provided that ceramic insulation is used and the coil casing cooling can accommodate 8 W/cm^3 by nuclear heating.[32] Because the ripple decays quickly away from the divertor, only a small region of the plasma ($\sim 2\ m^3$) experiences significant ripple ($>0.4\%$). Consequently, collisionless 150-keV D^+ ions are well confined in FED, except those with banana tips in the

high ripple region ($\geq$0.4%), which are lost. Fast ions resulting from near-tangential injection are expected to be well confined.

IV.C Discussion

The choice of the magnetic scrape-off thickness T_{so} must be justified, since the divertor coil currents (and consequent ripple) are an increasing function of T_{so}. As the scrape-off thickness increases, a larger current is required to form the separatrix, yielding a higher ripple. Using only step 1 (i.e., an unshielded, single-T divertor) of the optimization strategy (see Appendix), the resulting ripple in FED is 0.08% for T_{so} = 0.05 m, rising to 0.14% for T_{so} = 0.2 m (see Fig. 14). Inclusion of the back T-coil in the optimization decreases the ripple by a factor of 0.5 to 0.8 because the B-field of the back coil interferes destructively with that of the front coil. A value of T_{so} = 0.2 m was chosen for FED to provide an adequate scrape-off thickness while keeping the ripple below 0.3%.

The use of a single filament to model each leg of the divertor must also be checked against more realistic models. For example, each coil cross section can be represented by an N x N array of wire filaments for $1 \leq N \leq 4$. The maximum differences between the single filament case and multifilamentary cases in coil current, null position, and ripple are 2%, 6%, and 7%, respectively. This calculation was done with a field-line-plotting code[31] which can determine the magnetic configuration for divertor coils that are composed of straight-line filamentary wires. The corresponding result

for a uniform current density over the coil cross section gives slightly smaller differences compared to the single-filament case. This calculation relied on BARC13 (Ref. 33), which determines the magnetic configuration for coils of rectangular cross section having a homogenous current density. These small deviations confirm the validity of our model.

It is also appropriate to comment on a practical aspect of the T-coil design. If the "base" of the T-coil (the leg that lies along $\phi = 0$ in Fig. 13) has a rectangular copper cross section, the ripple is increased over a square (or circular cross-section) coil. This is because the more separated currents in the rectangular conductor are not as efficient in forming the field null as the square cross-section case. Consequently, more current is needed in the former case, yielding a higher ripple. On the other hand, if the base of the T-coil has a 1 x 1 square cross section, then the cross section in the front of the T-coil must be a 1/2 x 1 rectangle. This last situation appears to be practical[34] and is the one assumed in the present model for two reasons. First, the nulling fields are created only by the vertical filament in the base of the T-coil. Second, the front of the T-coil serves to create a high-order multiple magnetic moment, whose influence decreases quickly in moving away from the divertor.

V. CONCLUSIONS AND SUMMARY

Whereas divertor optimization is straightforward for present-day tokamaks, it is very difficult for reactors because there are stringent engineering trade-offs. Minimal power dissipation (and correspondingly low current) in the copper coils requires the divertor to be as close to the plasma as possible. However, the current (and concomitant ripple) necessary to join the separatrix to the plasma edge is a strong function of scrape-off region thickness. In addition, the diversion of enough particle and heat flux for adequate impurity control leads to a thicker scrape-off. In a reactor such a trade-off points toward reliance on the divertor as a means of impurity control and as a magnetic limiter, while increasing the risk inherent in such a design. Low ripple is another factor that may necessitate low divertor currents and plasma size optimization. Increasing the minor radius will move the magnetic axis away from the divertor, lowering the ripple. Decreasing the major radius (with B_o and minor plasma radius fixed) steepens the 1/R falloff in TF, also reducing ripple. An increase in minor radius must be balanced against larger cost, while a smaller major radius must be traded against space constraints for TF coils, structure, etc. While decreasing B_T and R_o and increasing the minor plasma radius may be advantageous for divertor design, it is beyond the scope of this work to assess the corresponding impact on plasma transport, reactor cost, etc.

Acceptable divertor configurations have been obtained for ETF/INTOR and FED. The size of the on-axis local ripple is a good quantitative indicator of the deleterious physics effects. Therefore, the divertor configuration is optimized to minimize ripple while satisfying an appropriate set of engineering constraints. Neutron shielding leads to a large divertor relatively far from the plasma edge, resulting in an unacceptably high ripple. An unshielded divertor allows for a smaller divertor that can fit between adjacent TF coiling, relatively close to the plasma, yielding acceptable ripple ($\delta < 0.3\%$). An unshielded divertor should suffice for a subignition ETF. Additional back coils are needed to expand the diverted flux bundle beyond the outer legs of the TF coiling so the heat flux to the collector plate is reduced to an acceptable level.

Implementation of a bundle divertor in a tokamak reactor remains a difficult problem. Experiments on DITE are continuing to yield important physics understanding, and ISX-B bundle divertor studies are expected to be under way early in 1982. These tests will not only explore the physics of impurity control but also examine the deleterious effects on the background plasma and fast ions. Even for an optimized divertor (whether shielded or unshielded), great care will be needed in the design of auxiliary heating systems. The cost of such systems is large, so that large losses of fast ions cannot be tolerated. Thus, it is necessary to evaluate the ripple-induced loss of energetic ions due to pitch angle scattering, as well as the loss of ion cyclotron resonant frequency-heated tail ions. Although this presents a somewhat gloomy picture, recent calculations[35] of the ignition margin in ETF have shed a very positive light on this problem.

All the banana-trapped, 150-keV, neutral-injected deuterons were assumed to be lost with a local trapping fraction of $\sqrt{2r/R}$, yielding a 50% net D^+ loss without pitch-angle scattering. The resulting decrease in ion temperature causes lower ripple-trapping losses from the background plasma with only a 20% drop in fusion power. Although the net alpha power deposition in the plasma decreases by 60%, ignition is still maintained. This is a hopeful sign that it is possible (though difficult) to design a bundle divertor for a tokamak reactor.

ACKNOWLEDGMENTS

Fruitful discussions with J. Sheffield and T. F. Yang (MIT) are acknowledged with thanks. We are grateful to S. S. Kalsi [Fusion Engineering Design Center (FEDC)/General Electric] for performing the BARC13 calculations and to P. H. Sager (FEDC/General Atomic) for evaluating the neutron damage effects for an unshielded divertor. We also thank C. Ruchti (Cornell University) for developing the divertor field-line-plotting code FLP for our use.

APPENDIX

DIVERTOR OPTIMIZATION TECHNIQUE

The constrained optimization algorithm is illustrated in Fig. A.1. The numerical search begins with a user-supplied guess for the optimal configuration. Given this configuration, it is necessary to find the coil currents so that the separatrix joins the plasma edge far from the divertor. This part of the algorithm is shown inside the dashed box of Fig. A.1. After the coil currents are picked, a numerical search is used to find the null in B_ϕ along the line $\phi = 0$, $z = 0$. Equation (9) is then used to integrate the $\vec{B}$-line from the null to the plasma edge. If the separatrix does not join the plasma edge within the required tolerance, a new set of coil currents is chosen, and the above process is repeated.

From the currents I_1 and I_2 in the front and back T-coils, respectively ($r = I_2/I_1$), the radius of the copper coils is determined from the power dissipation restriction

$$(r_{cu})_p = I_1 \left[\frac{\rho(\ell_1 + r^2 \ell_2)}{\pi f_{pk} P} \right]^{1/2} \qquad (A.1)$$

and from the current density constraint

$$(r_{cu})_c = \left(\frac{I_1}{\pi J} \right)^{1/2} , \qquad (A.2)$$

where $\ell_1 = 4(L_1 + D_1 + H_1)$ and $\ell_2 = 4(L_2 + D_2 + H_2)$ as indicated in Fig. 13. Combining Eqs. (A.1) and (A.2) yields the coil radius according to the more restrictive constraint

$$r_{cu} = \max\left[(r_{cu})_c, (r_{cu})_p\right] . \tag{A.3}$$

From the radius of the copper coils, the constraints can be found. An adequate hole through the front bore of the coils is required:

$$\delta L_1 = 2L_1 - X_h - 2r_{cu} - 2S_f \geq 0 . \tag{A.4}$$

The hole through the side of the T-coils must also be large enough:

$$\delta D_1 = \left(L_1^2 + D_1^2\right)^{1/2} - X_h - S_f - S_b - (1 + \sqrt{2})r_{cu} \geq 0 . \tag{A.5}$$

The vertical hole size cannot be too small:

$$\delta H_1 = H_1 - Y_h - 2\sqrt{2}\ r_{cu} - 2S_f \geq 0 . \tag{A.6}$$

The constraints δL_2, δD_2, and δH_2 are similarly defined for the back T-coil, which has a cross-sectional radius of $\sqrt{r}\ r_{cu}$. The front of the inner T-coil must lie outside the plasma scrape-off region:

$$\delta R_1 = R_1 - (R_{edge} + T_{so} + S_f + r_{cu}) \geq 0 , \tag{A.7}$$

where R_{edge} is the outboard major radius of the plasma. The front of the outer T-coil cannot interfere with the back of the inner T-coil:

$$\delta R_2 = R_2 - [R_1 + D_1 + (\sqrt{r} + \sqrt{2})r_{cu} + S_f + S_b] \geq 0 . \qquad (A.8)$$

Finally, the flux bundle must be expanded through the outer T-coil:

$$\delta R_{sep} = R_{sep}^{max} - (R_2 + D_2 + \sqrt{2}\, r\, r_{cu} + S_b) \geq 0 , \qquad (A.9)$$

where R_{sep}^{max} is the maximum major radius of the separatrix, obtained by integrating Eq. (9) from the B_ϕ null through the divertor.

Parameter studies of the double-T divertor yield the following optimization strategy:

(1) Optimize the front T-coil in accordance with the above constraints with the back T-coil (farthest from plasma) turned off (since the front coil contributes most of the ripple) where

   a. the smallest value of R_1 is used, so that $\delta R_1 = 0$ (consistent with the findings of Ref. 6);

   b. the smallest values of D_1 and H_1 are used so that $\delta D_1 = 0$ and $\delta H_1 = 0$, since the ripple increases monotonically with coil size;

   c. the flux bundle circles around the outboard side of the outer filament of the front T-coil so the back T-coil can then expand the flux bundle, i.e.,

$$\delta R_{sep} = R_{sep}^{max} - (R_1 + D_1) \geq 0 .$$

(2) Optimize both the back and front T-coils subject to the above restrictions, with the result of step 1 as the starting point for step 2; in addition,

   a. the smallest value of R_2 is used, so that $\delta R_2 = 0$;

b. the flux bundle lies just beyond the back T-coil, so that $\delta R_{sep} = 0$.

(3) Include discrete TF ripple effects, since expansion of the flux bundle becomes easier if the back T-coil extends outside the TF coils.

(4) Confirm the fast ion confinement with FLOC calculations.[17]

The objective function to be minimized is the on-axis ripple, subject to the constraints in Eqs (A.1) through (A.9). This constrained minimization search is performed by the Numerical Algorithms Group routine,[36] E04UAF, which uses an augmented Lagrangian method to satisfy the constraints and a quasi-Newton's method to minimize δ. Steps 1 and 2 of the above optimization strategy typically require 1 to 2 central processing unit hours on a CDC-7600.

Several of the examples discussed in Sec. IV.D are given in Table A.I.

TABLE A.I. OPTIMIZED DIVERTOR PARAMETERS

Parameter	ISX-B	FED
R_o (m)	0.935	5.00
R_{edge} (m)	1.18	6.08
a (m)	0.25	1.30
b/a	1.17	1.60
q_s	6.0	2.6
I_{pl} (MA)	0.15	6.20
β_p	0.51	1.50
B_o (T)	1.80	3.60
		Unshielded
R_1 (m)	1.277	6.319
L_1 (m)	0.192	0.353
D_1 (m)	0.242	0.442
H_1 (m)	0.197	0.711
R_2 (m)	0.594	7.010
L_2 (m)	0.237	1.096
D_2 (m)	0.013	0.350
H_2 (m)	0.197	1.050
I_1 (MA)	0.223	2.276
I_2/I_1	.9	0.718
δ (%)	0.343[a]	0.084
r_{cu} (m)	0.034	0.110

[a]Value when TF ripple is not included; δ = 0.21% with TF ripple, caused by destructive interference between the TF and divertor fields.

REFERENCES

[1] P. E. STOTT, C. M. WILSON, and A. GIBSON, Nucl. Fusion 17, 481 (1977).

[2] P. E. STOTT, C. M. WILSON, and A. GIBSON, Nucl. Fusion 18, 475 (1978).

[3] D. MEADE, V. ARUNASALAM, C. BARNES, M. BELL, M. BITTER, et al., in Plasma Physics and Controlled Nuclear Fusion Research (Proc. 8th Int. Conf., Brussels, 1980), Vol. 1, 665, IAEA, Vienna (1980).

[4] M. KEILHACKER, D. B. ALBERT, K. BEHRINGER, R. BEHRISCH, W. ENGELHARDT, et al., in Plasma Physics and Controlled Nuclear Fusion Research (Proc. 8th Int. Conf., Brussels, 1980), Vol. 2, 351, IAEA, Vienna (1980).

[5] T. F. YANG, G. W. RUCK, A. Y. LEE, G. SMETZLER, and T. PREVENSLIK, Westinghouse Electric Corporation Rep. WFPS-TME-104 (November 1978).

[6] C. COLVEN, A. GIBSON, and P. E. STOTT, in Controlled Fusion and Plasma Physics (Proc. 5th European Conf., Grenoble, France, 1972), Vol. 1, 6, IAEA, Vienna (1972).

[7] P. J. HARBOUR, M. F. A. HARRISON, A. D. SANDERSON, and P. E. STOTT, in Plasma Physics and Controlled Nuclear Fusion Research (Proc. 5th Int. Conf., Innsbruck, 1978), Vol. 1, 431, IAEA, Vienna (1978).

[8] R. B. WYSOR, T. C. JERNIGAN, W. R. WING, B. E. NELSON, D. H. GRAY, et al., in Engineering Problems of Fusion Research

(Proc. 8th Symp., San Francisco, California, 1979), Vol. 2, 1337 (1979).

[9] T. F. YANG, A. Y. LEE, G. W. RUCK, T. V. PREVENSLIK, and G. SMETZLER, in Engineering Problems of Fusion Research (Proc. 8th Symp., San Francisco, California), Vol. 2, 615 (1979).

[10] G. M. SWIFT and F. H. SOUTHWORTH, in Engineering Problems of Fusion Research (Proc. 7th Symp., Knoxville, Tennessee, 1977), Vol. 2, 1198 (1977).

[11] "International Tokamak Reactor: Zero Phase," IAEA, Vienna, 145-147 (1980).

[12] R. A. DORY, R. B. EASTER, R. H. FOWLER, W. H. GRAY, H. C. HOWE, et al., "Bundle Divertor Research at ORNL," presented at the U.S./Japan Seminar, Tokyo, paper 4-4 (1980).

[13] J. W. CONNOR and R. J. HASTIE, Nucl. Fusion 13, 221 (1973).

[14] J. N. DAVIDSON, Nucl. Fusion 16, 731 (1976).

[15] N. A. UCKAN, T. UCKAN, and J. R. MOORE, Oak Ridge National Laboratory Rep. ORNL/TM-5603 (September 1976).

[16] K. T. TSANG, Nucl. Fusion 17, 557 (1977).

[17] R. H. FOWLER, D. K. LEE, P. W. GAFFNEY, and J. A. ROME, Oak Ridge National Laboratory Rep. ORNL/TM-6293 (June 1978).

[18] R. J. GOLDSTON, D. L. JASSBY, H. H. TOWNER, R. H. FOWLER, J. F. LYON, et al., in Engineering Problems of Fusion Research (Proc. 7th Symp., Knoxville, Tennessee, 1977), Vol. 2, 1333 (1977).

[19] R. J. GOLDSTON and D. L. JASSBY, Princeton Plasma Physics Laboratory Rep. MATT-1244 (May 1976).

[20] R. J. GOLDSTON and H. H. TOWNER, Princeton Plasma Physics Laboratory Rep. PPPL-1637 (February 1980).

[21] K. TANI, H. KISHIMOTO, and S. TAMURA, in Plasma Physics and Controlled Nuclear Fusion Research (Proc. 8th Int. Conf., Brussels, 1980), IAEA, Vienna (1980).

[22] R. H. FOWLER, J. A. ROME, D. J. STRICKLER, and J. F. LYON, Bull. Am. Phys. Soc. 24, 993 (1979).

[23] J. A. ROME, R. H. FOWLER, V. E. LYNCH, and J. F. LYON, Bull. Am. Phys. Soc. 24, 1045 (1979).

[24] R. J. GOLDSTON, Bull. Am. Phys. Soc. 24, 1094 (1979).

[25] W. STODIEK, K. BOL, H. EUBANK, S. VON. GOELER, and D. J. GROVE, Princeton Plasma Physics Laboratory Rep. MATT-853 (July 1971).

[26] G. BATEMAN and R. N. MORRIS, Georgia Institute of Technology Fusion Research Rep. GTFR-15 (May 1980).

[27] S. K. ERENTS, S. J. FIELDING, R. D. GILL, D. H. J. GOODALL, J. HUGILL, et al., in Plasma Physics and Controlled Nuclear Fusion Research (Proc. 8th Int. Conf., Brussels, 1980), IAEA, Vienna (1980).

[28] R. C. ISLER, S. L. MILORA, D. E. ARNURIUS, S. C. BATES, K. H. BURRELL, et al., in Plasma Physics and Controlled Nuclear Fusion Research (Proc. 8th Int. Conf., Brussels, 1980); IAEA, Vienna (1980); S. D. SCOTT, Ph.D. Thesis (MIT) 1982.

[29] J. A. ROME and Y-K. M. PENG, Nucl. Fusion 19, 1193 (1979).

[30] R. H. FOWLER, J. A. HOLMES, and J. A. ROME, Oak Ridge National Laboratory Rep. ORNL/TM-6845 (July 1979).

[31] C. RUCHTI, Oak Ridge National Laboratory Rep. ORNL/TM-7555 (January 1981).

[32] P. H. SAGER, General Atomic Company, private communication (October 1980).

[33] J. C. WHITSON and W. I. VAN RIJ, J. Appl. Phys. 47, 3291 (1976).

[34] S. S. KALSI, General Electric, private communication (November 7, 1980).

[35] W. A. HOULBERG, Oak Ridge National Laboratory, private communication (December 11, 1980).

[36] Numerical Algorithms (USA) Group, Inc., 1250 Grace Court, Downers Grove, Illinois 60515, U.S.A. (Edition 8).

FIGURE CAPTIONS

FIG. 1. Flux surfaces ETF/INTOR with a four-coil bundle divertor. The same base equilibrium has been used with different edge safety factors. On the left, $q_{edge} = 2$ allows large $m = 2$ islands to interact with the divertor field and produce ergodic flux surfaces. On the right, $q_{edge} = 4$ and the flux surfaces are well formed.

FIG. 2. The projection at a constant toroidal angle of a guiding-center orbit for an ion that becomes trapped between the maximum in B produced by the divertor and the usual 1/R decrease in B. The example shown is for an alpha particle in a low beta ($\beta = 0.6\%$) ETF/INTOR equilibrium whose poloidal flux surfaces are indicated by the dotted contours.

FIG. 3. The orbit of an alpha particle that drifts to the wall because its banana tips are displaced by encounters with the divertor ripple. The equilibrium used is the same as that in Fig. 2.

FIG. 4. Orbit (a) for a trapped alpha particle (top) in ETF. P_ϕ changes randomly (b), indicating that the ion is walking out. The corresponding Poincaré puncture plot (where each point indicates where the guiding-center orbit intersects the $\phi = 180^o$ plane) is ergodic (c). The position of the double-T divertor relative to the plasma is also shown.

FIG. 5. Circulating alpha orbit (a) in ETF. The P_ϕ is strikingly periodic (b), indicating that a new invariant of the motion exists. The corresponding Poincaré puncture plot has well-formed islands (c), meaning that the particle is well contained.

FIG. 6. Contours of B = 4.8 T at various toroidal angles relative to

the vertical symmetry plane of a two-coil ETF/INTOR divertor (a). When the contours in (a) are combined in three dimensions, (b) is obtained; similarly, for other values of total field (c) and (d). Because the equilibrium is for high beta, closed toroidal B surfaces exist and may become pinched off due to the fields of the divertor.

FIG. 7. Three different B = constant surfaces for a four-coil ETF/INTOR divertor. This configuration has been chosen to minimize any maxima in B created by the divertor.

FIG. 8. The ISX-B bundle divertor and three of the resulting B surfaces. For this low beta equilibrium, the B surfaces would be nearly concentric cylinders if there was no divertor.

FIG. 9. Ripple contours (dotted) for the ISX-B divertor, obtained by evaluating B along each line of R = constant and z = constant without plasma current.

FIG. 10. The map of field lines from the symmetry plane of the divertor (in the collector region) into the tokamak, going 45° in the toroidal direction. For example, the field line beginning at point A in the collector region maps to point A in the plasma; the same correspondence applies to point B, B′, etc. There is a one-to-one mapping between intermediate unlabelled points as well. The vertical displacement is due to the rotational transform.

FIG. 11. Summary of containment for collisionless 40-keV protons in a low beta, ISX-B plasma. The letter designations are as follows: C — contained, D — diverted (hit collector), M — mirrored by divertor field (missed collector), E — ergodic, L — lost (hit wall). Here ψ_x is the maximum value of the poloidal flux function along the orbit, normalized

to the value of ψ at the plasma edge; $\zeta = v_{\parallel}/v$ at ψ_x, where v is the particle speed and $\zeta > 0$ corresponds to cogoing ion orbits.

FIG. 12. The birth points of beam ions derived using a Monte Carlo beam deposition code (see Ref. 30). Most beam ions are born outside the trapped particle region in ISX-B.

FIG. 13. Geometry of the double-T divertor (illustrated in Figs. 4 and 5), labeled to show optimizable parameters. Not shown are H_1 and H_2, the heights of the front and back T-coils, respectively.

FIG. 14. On-axis ripple for optimal T-coil divertors on FED. The magnetic scrape-off thickness is T_{so}. Curve (a) refers to ripple vs T_{so} for optimal, double-T divertors with a bore width/height of 0.3/0.4 m; curve (b) refers to optimal single-T divertors with a bore width/height of 0.5/0.6 m (see text).

Fig. A.1. Constrained optimization algorithm.

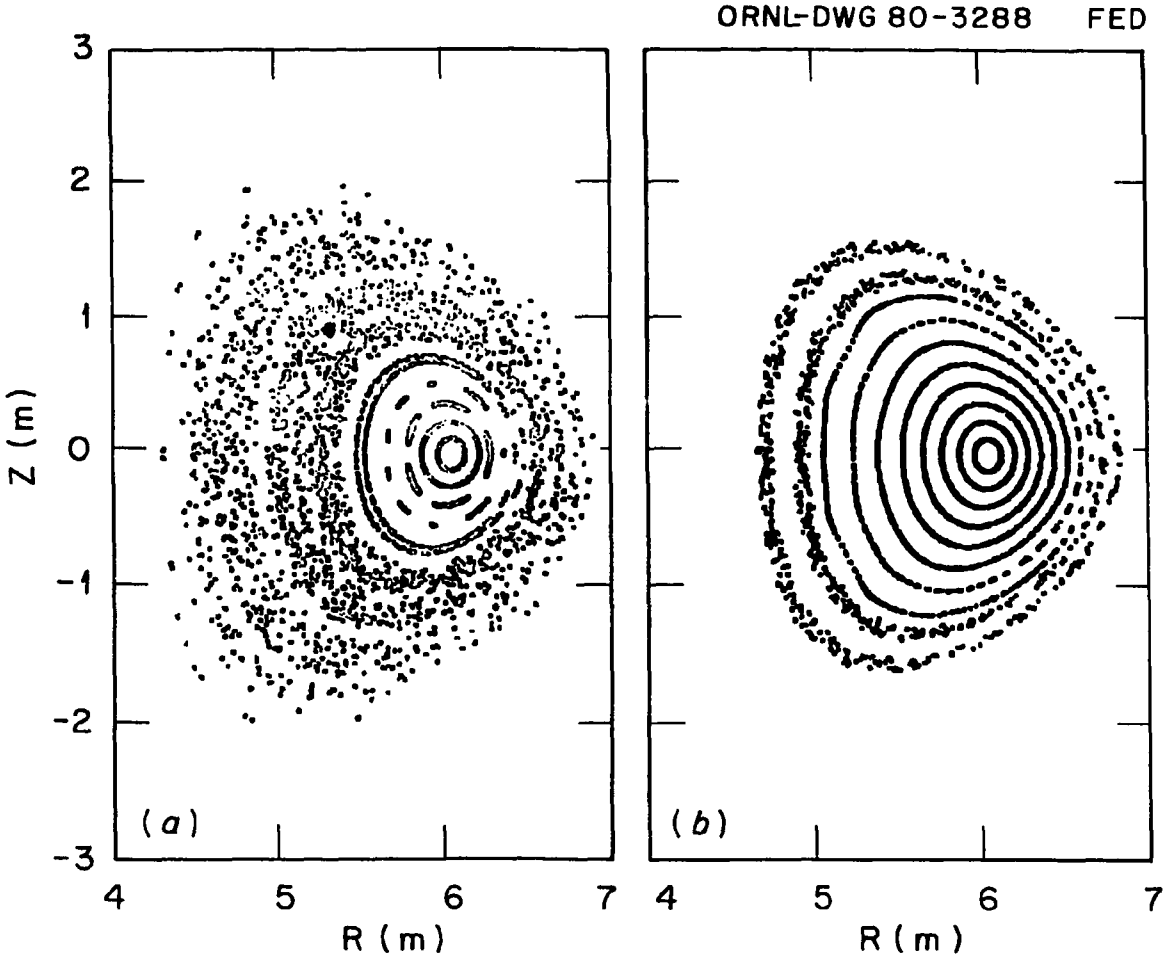

Fig. 1

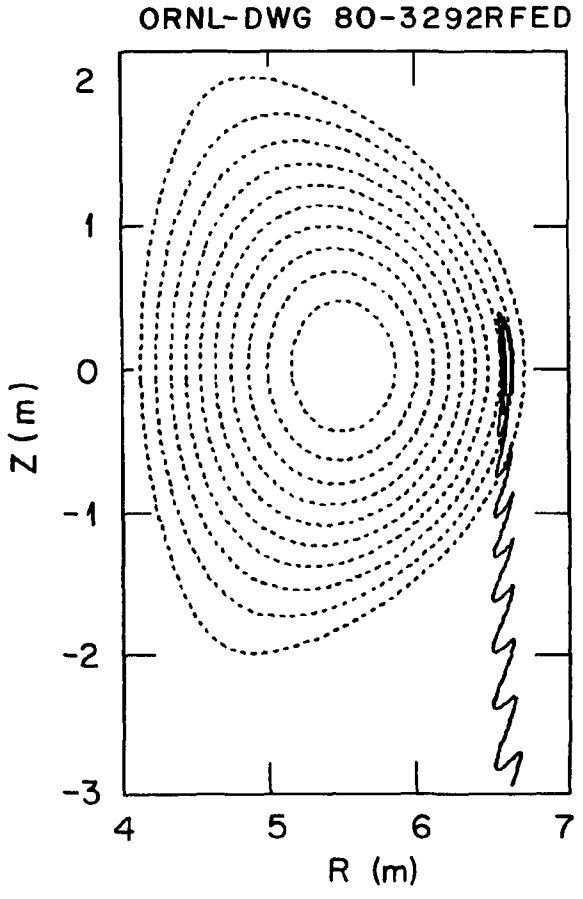

Fig. 2

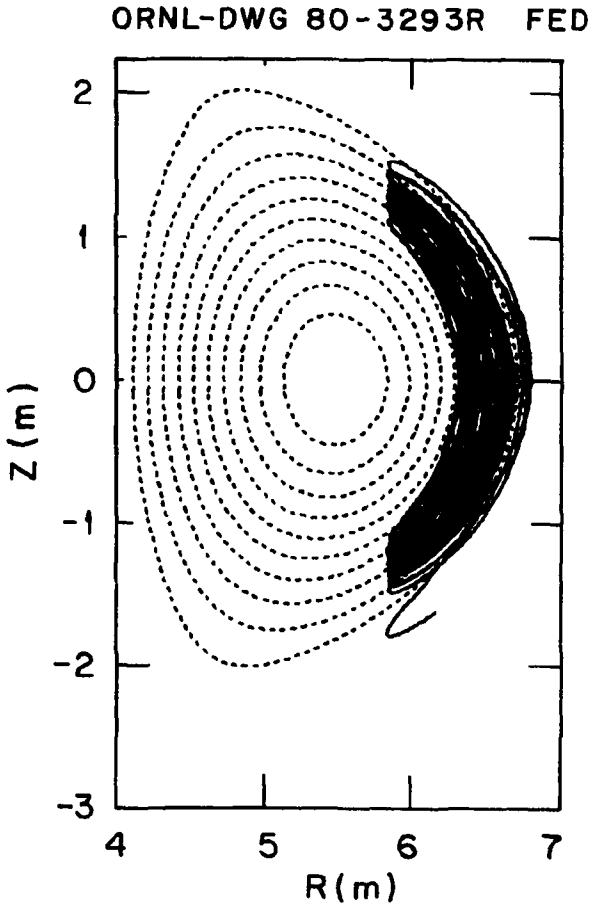

Fig. 3

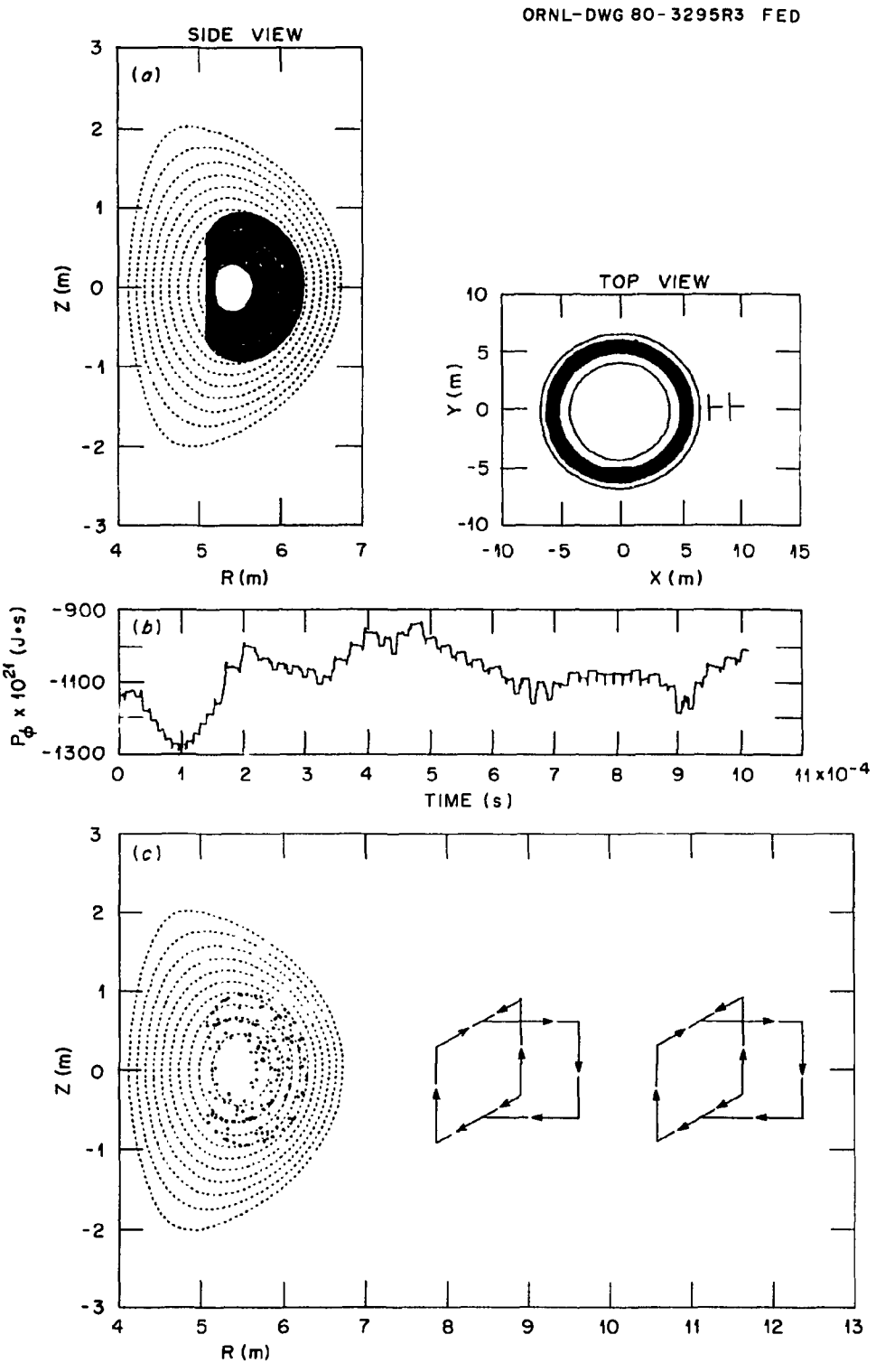
ORNL-DWG 80-3295R3 FED
SIDE VIEW
(a)
Z (m)
R (m)
TOP VIEW
Y (m)
X (m)
(b)
$P_\phi \times 10^{21}$ (J•s)
TIME (s)
11 x10^{-4}
(c)
Z (m)
R (m)

Fig. 4

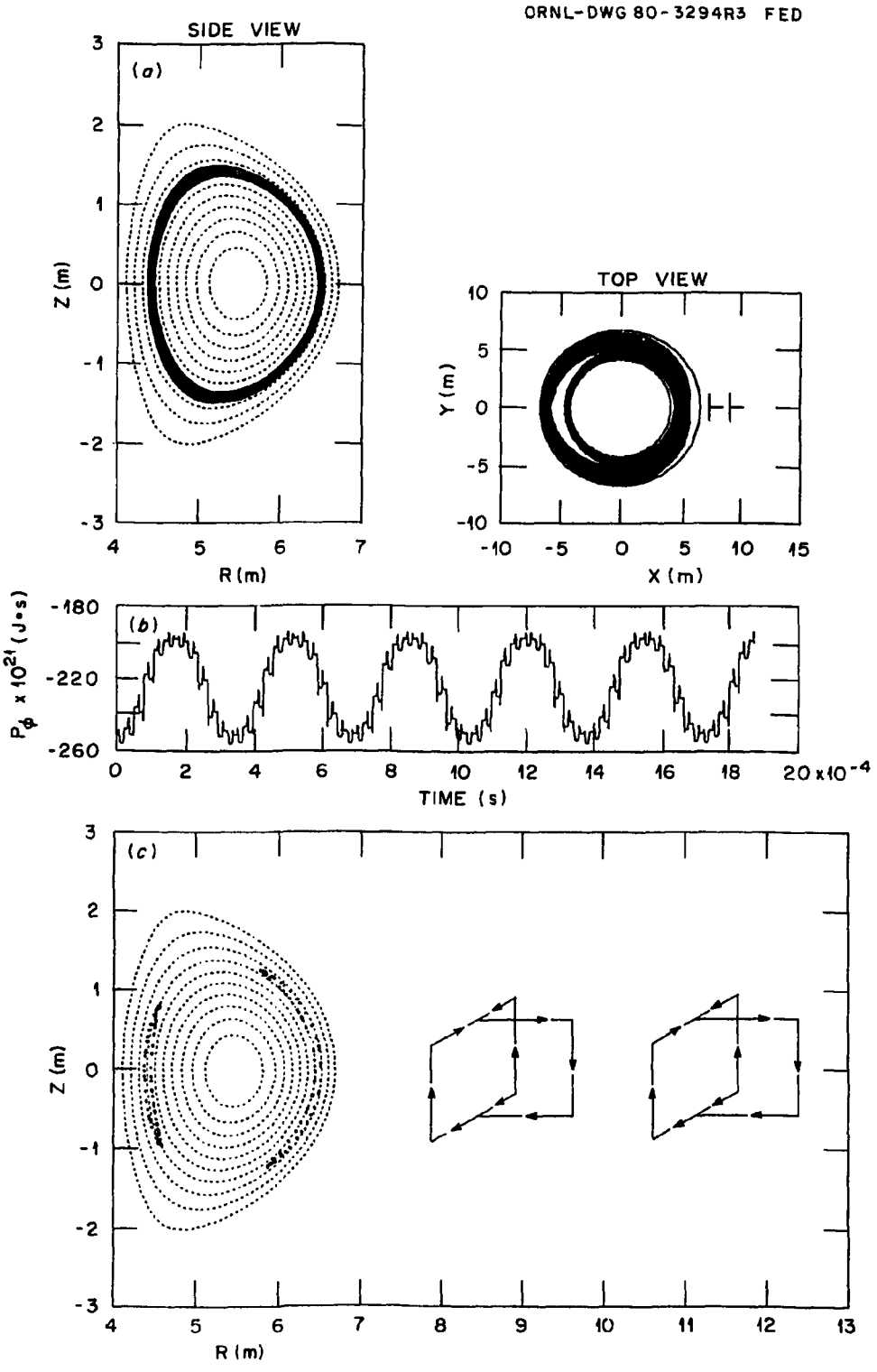
ORNL-DWG 80-3294R3 FED
SIDE VIEW
(a)
Z (m)
R (m)
TOP VIEW
Y (m)
X (m)
(b)
$P_\phi \times 10^{21}$ (J•s)
TIME (s)
20 x10^{-4}
(c)
Z (m)
R (m)

Fig. 5

ORNL-DWG 80-3291R3 FED

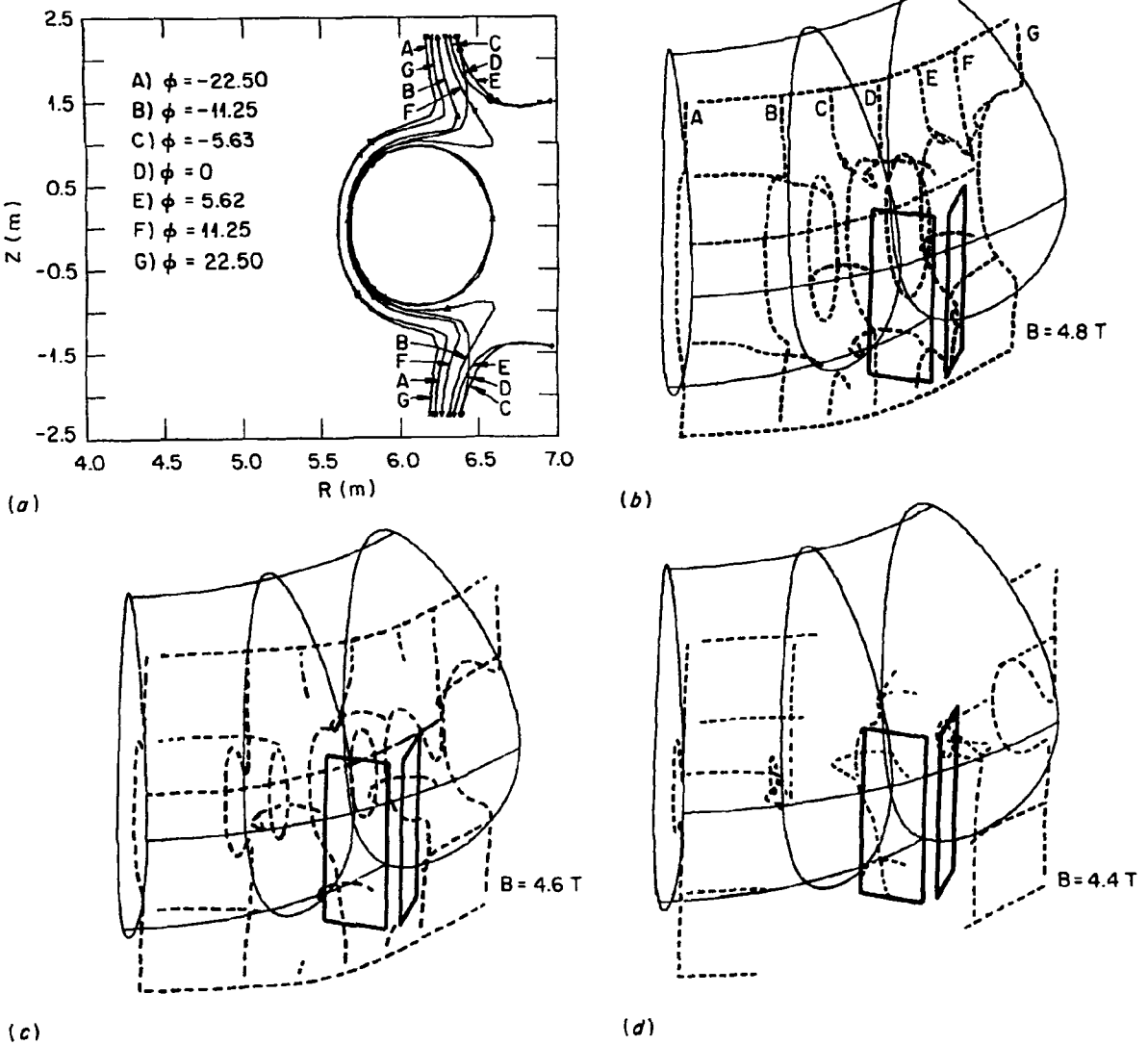

Fig. 6

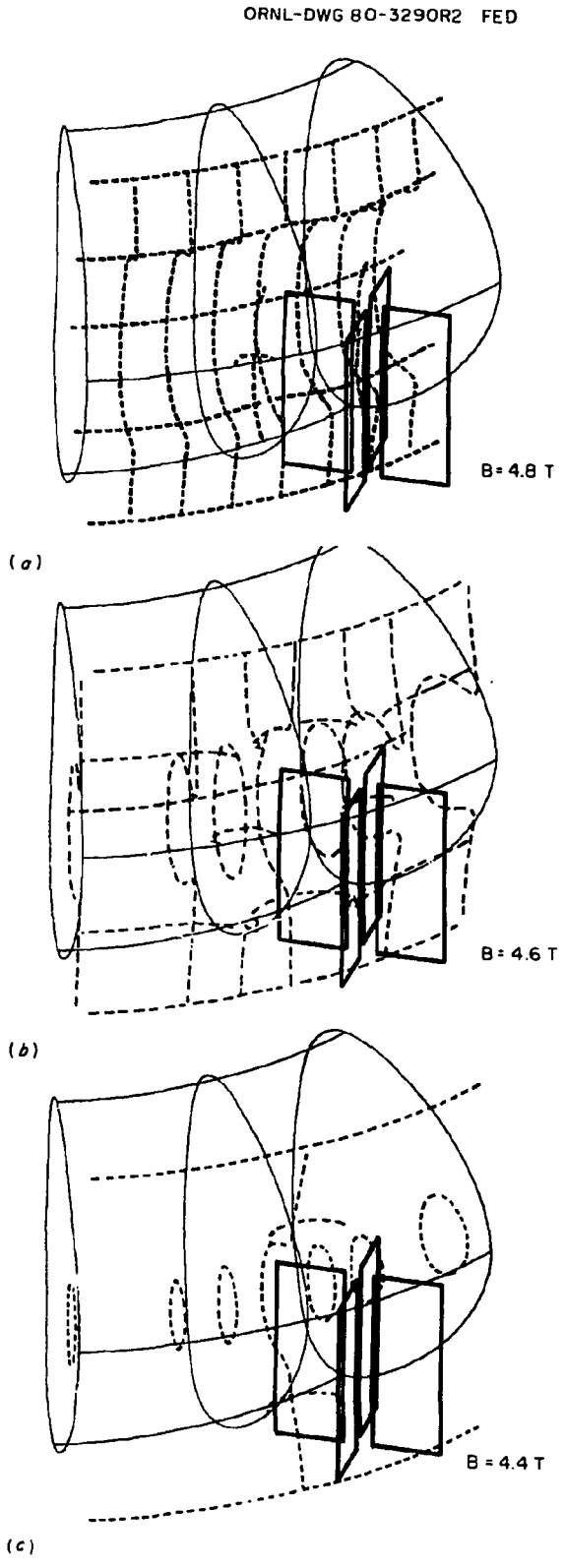

Fig. 7

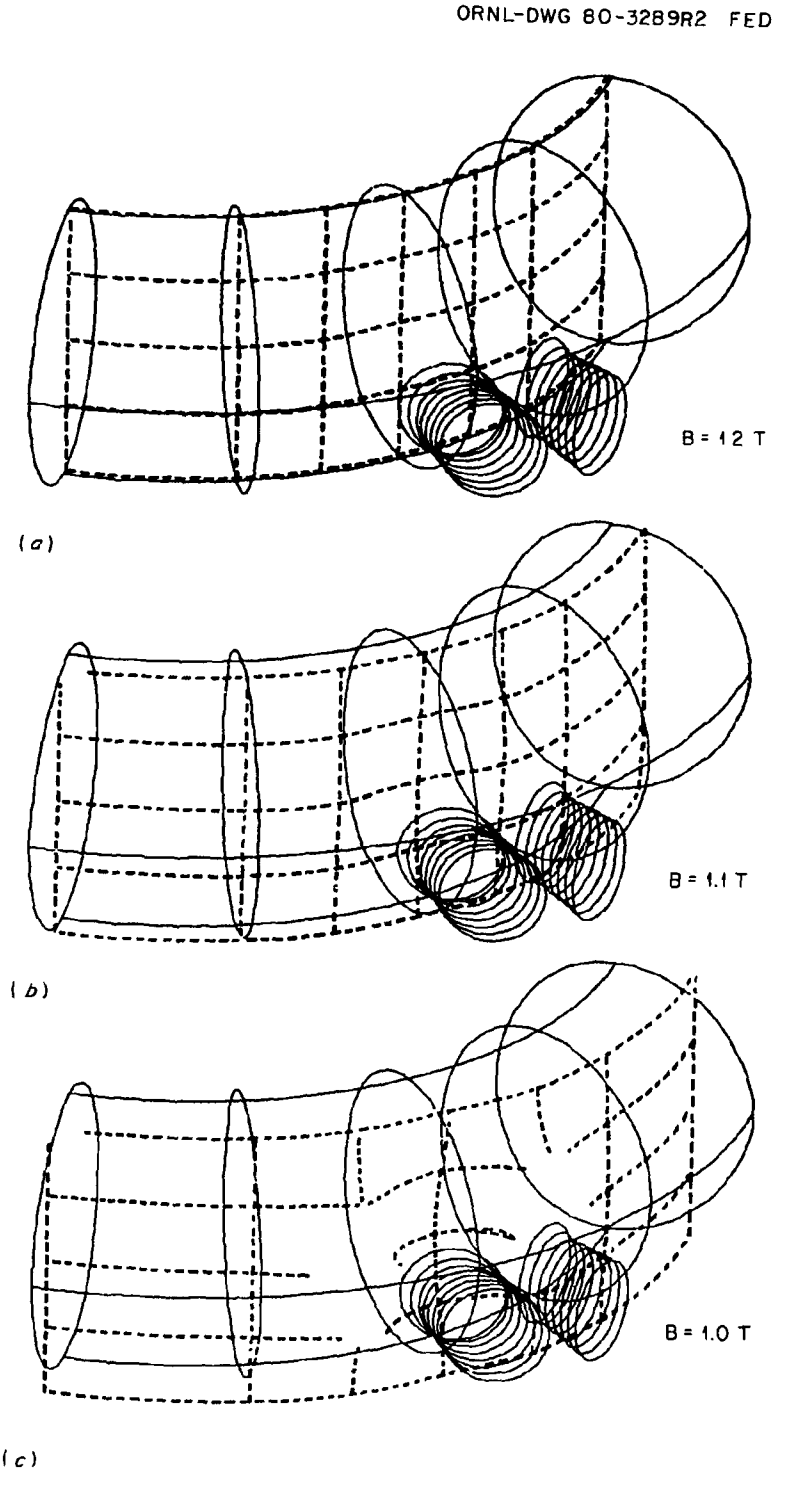

Fig. 8

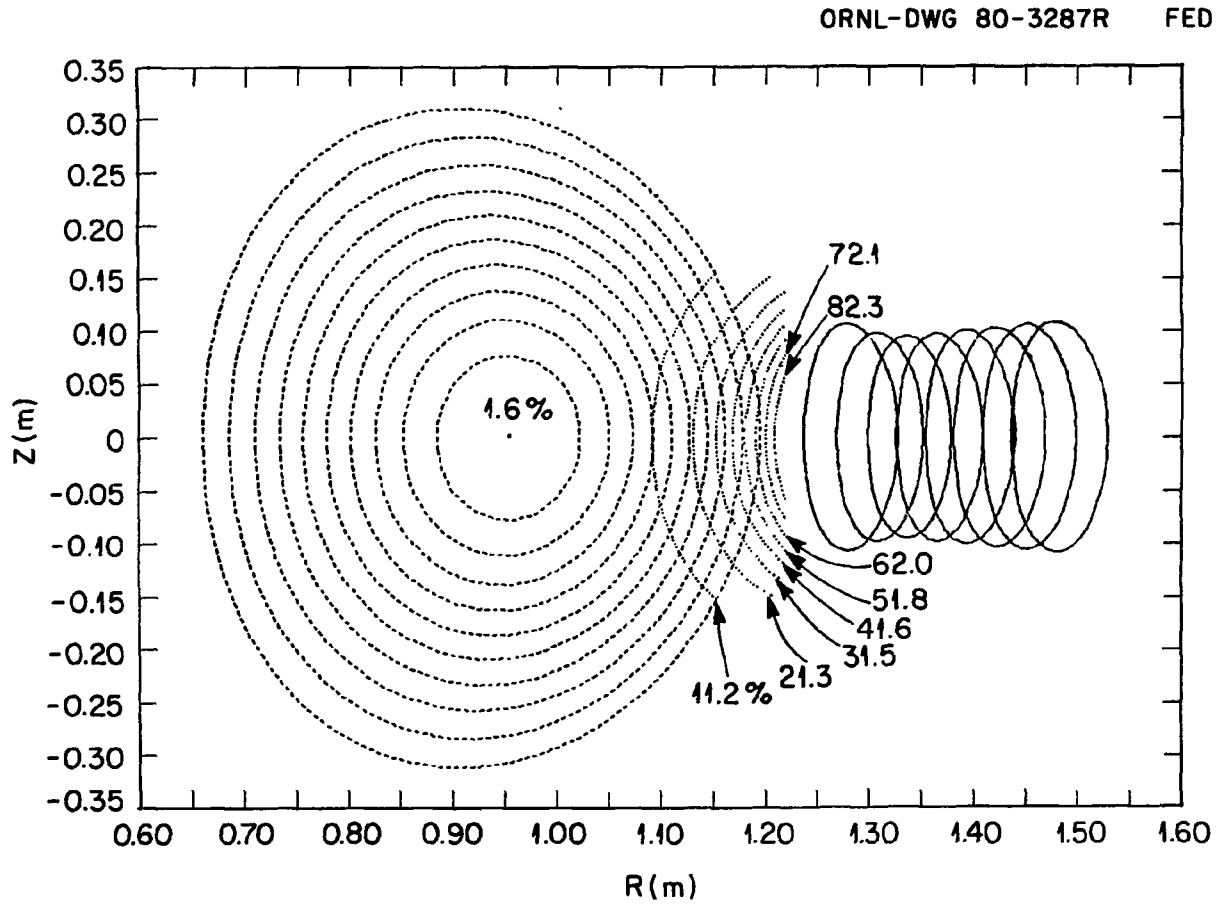
ORNL-DWG 80-3287R FED
0.35
0.30
0.25
0.20
0.15
0.10
0.05
0
-0.05
-0.10
-0.15
-0.20
-0.25
-0.30
-0.35
Z(m)
0.60
0.70
0.80
0.90
1.00
1.10
1.20
1.30
1.40
1.50
1.60
R(m)
1.6%
11.2%
72.1
82.3
62.0
51.8
41.6
31.5
21.3

Fig. 9

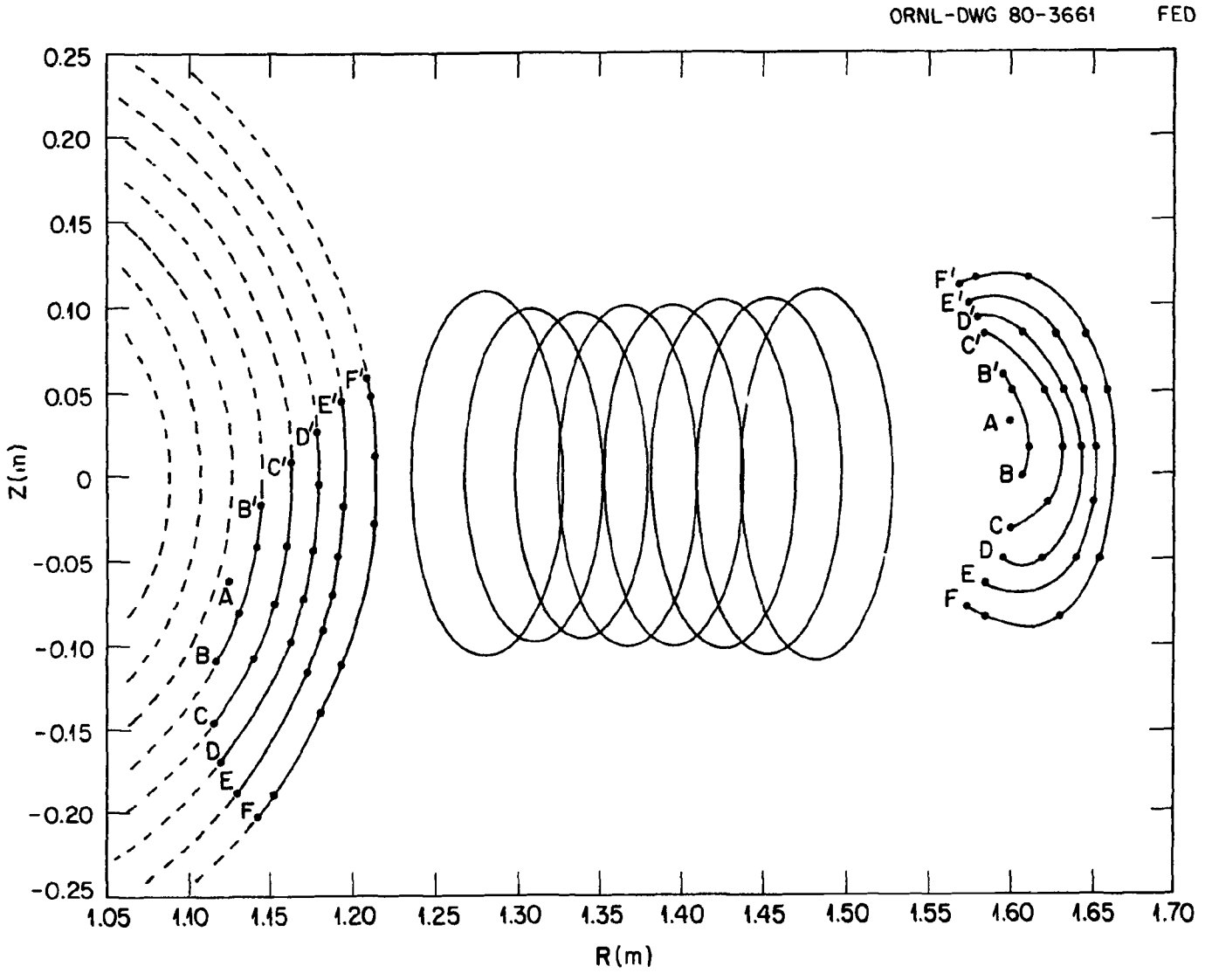
ORNL-DWG 80-3661 FED
0.25
0.20
0.15
0.10
0.05
0
-0.05
-0.10
-0.15
-0.20
-0.25
Z(m)
1.05
1.10
1.15
1.20
1.25
1.30
1.35
1.40
1.45
1.50
1.55
1.60
1.65
1.70
R(m)
A
B
C
D
E
F
B′
C′
D′
E′
F′

Fig. 10

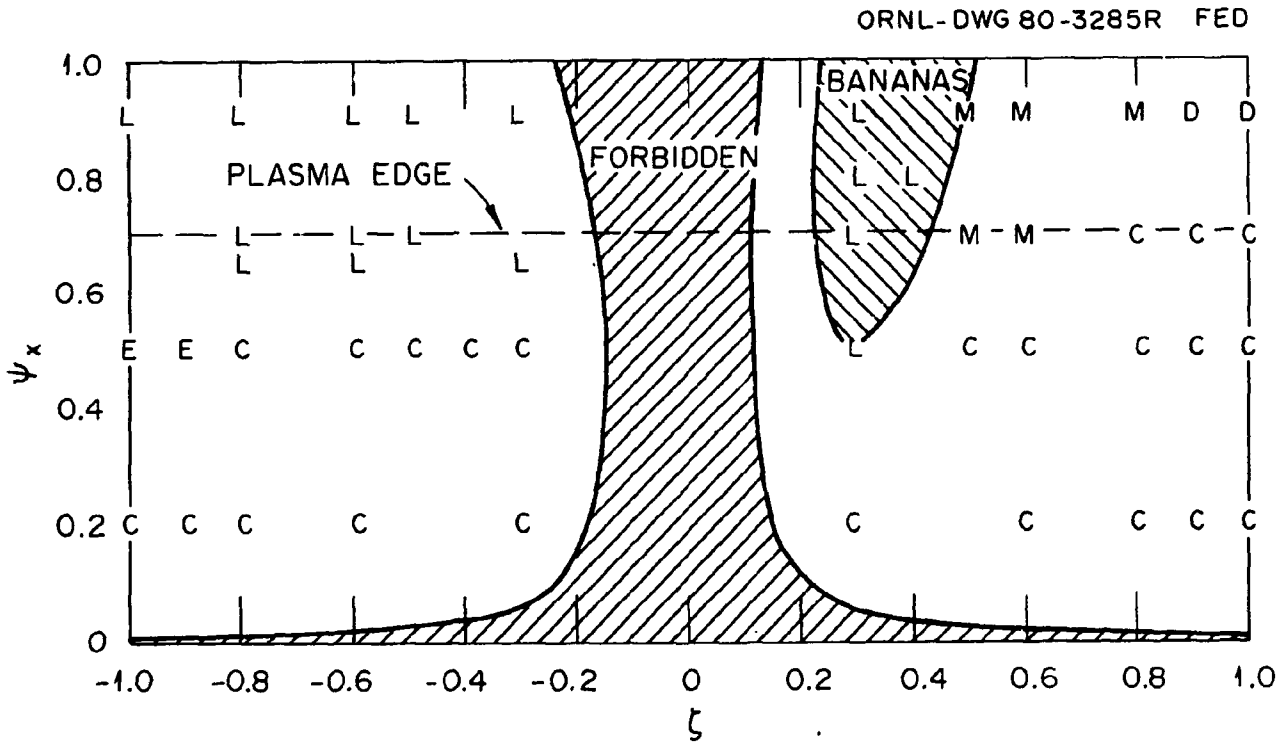
ORNL-DWG 80-3285R FED
BANANAS
FORBIDDEN
PLASMA EDGE
1.0
0.8
0.6
0.4
0.2
0
ψ_x
-1.0
-0.8
-0.6
-0.4
-0.2
0
0.2
0.4
0.6
0.8
1.0
ζ

Fig. 11

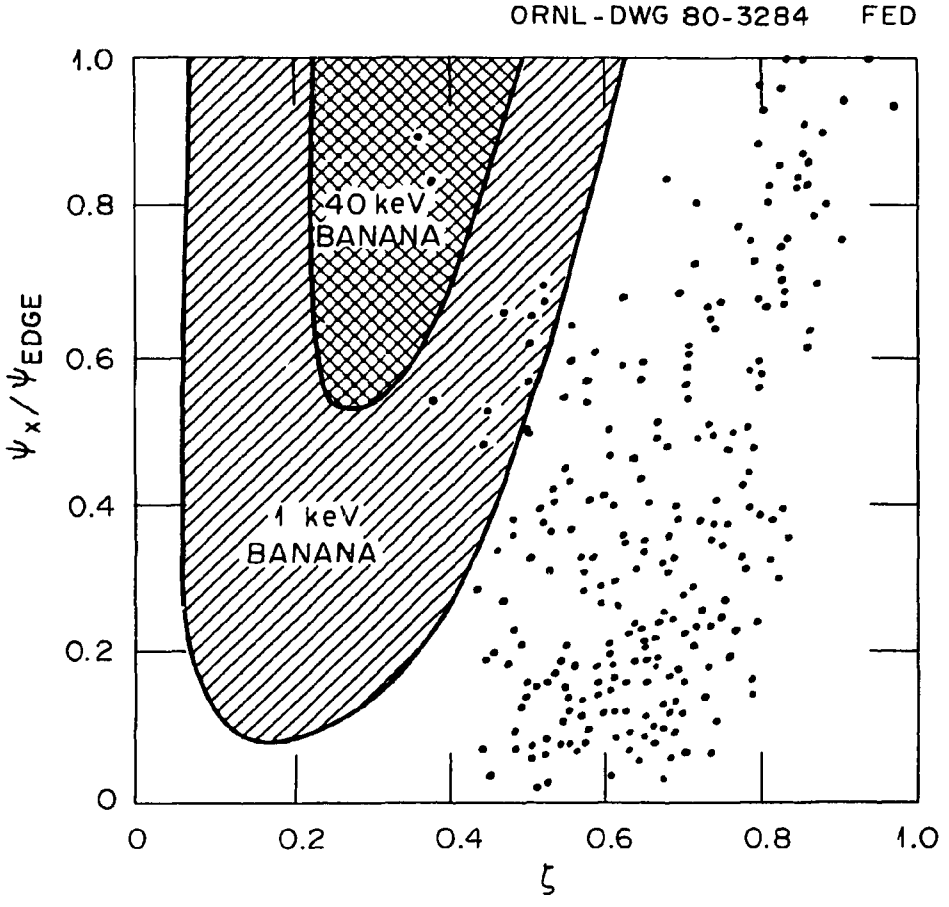
ORNL-DWG 80-3284 FED
1.0
0.8
0.6
0.4
0.2
0
ψ_x / ψ_{EDGE}
40 keV BANANA
1 keV BANANA
0
0.2
0.4
0.6
0.8
1.0
ζ

Fig. 12

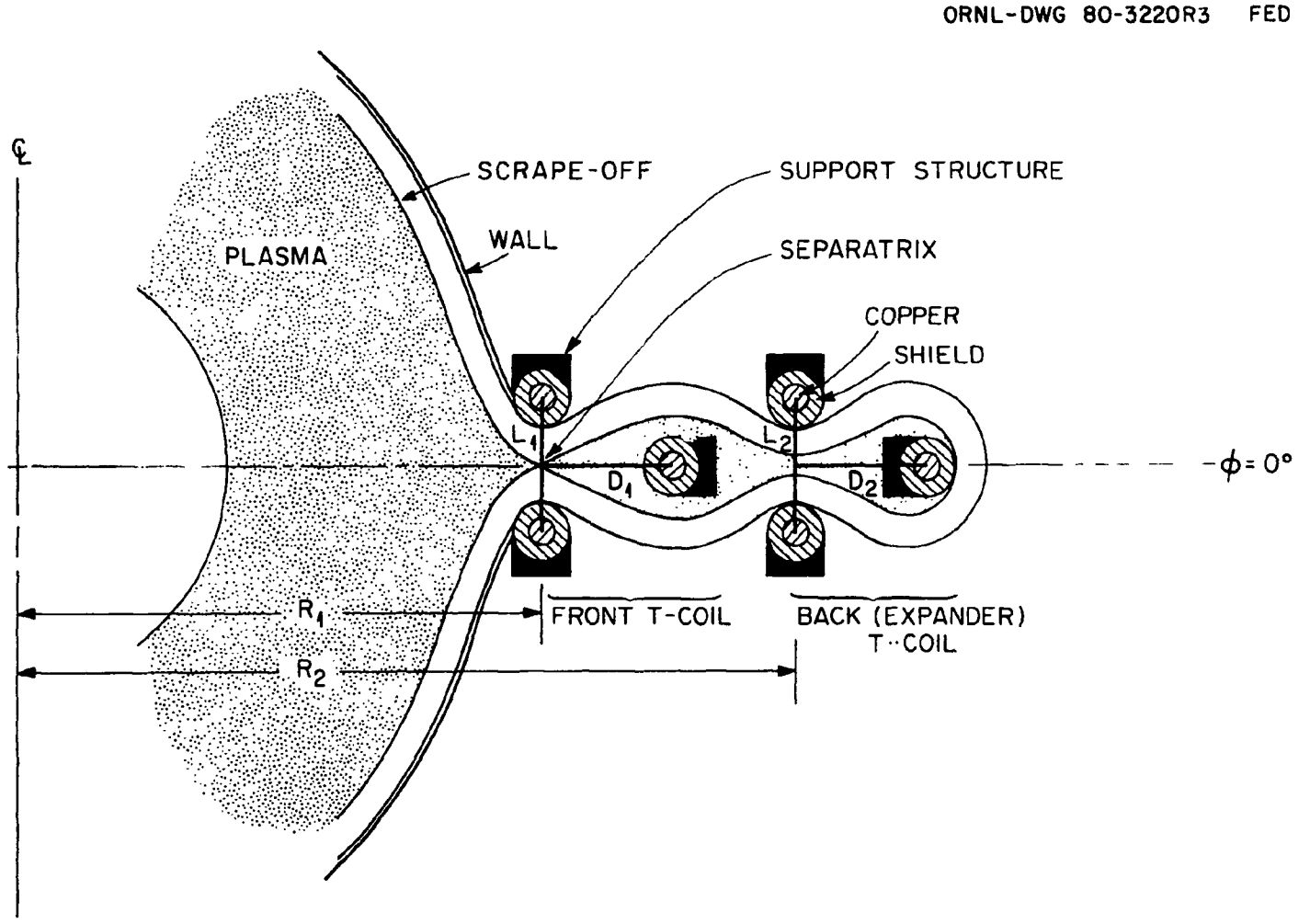
ORNL-DWG 80-3220R3 FED
℄
SCRAPE-OFF
SUPPORT STRUCTURE
WALL
SEPARATRIX
PLASMA
COPPER
SHIELD
L1
L2
D1
D2
-ϕ = 0°
R1
R2
FRONT T-COIL
BACK (EXPANDER)
T-COIL

Fig. 13

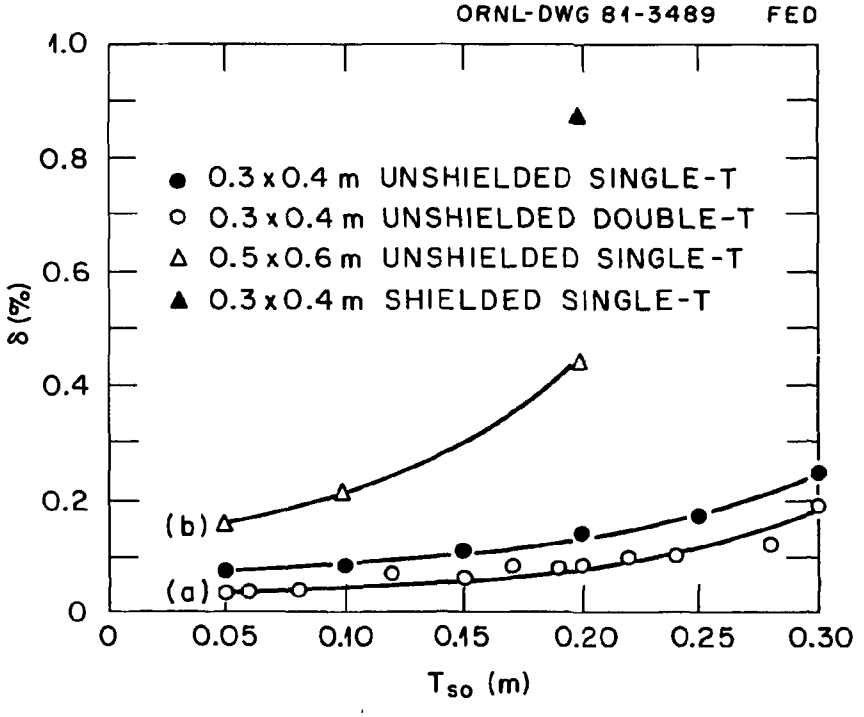
ORNL-DWG 81-3489 FED
1.0
0.8
0.6
0.4
0.2
0
δ (%)
● 0.3 x 0.4 m UNSHIELDED SINGLE-T
○ 0.3 x 0.4 m UNSHIELDED DOUBLE-T
△ 0.5 x 0.6 m UNSHIELDED SINGLE-T
▲ 0.3 x 0.4 m SHIELDED SINGLE-T
(b)
(a)
0
0.05
0.10
0.15
0.20
0.25
0.30
Tso (m)

Fig. 14

ORNL-DWG 80-3219 FED

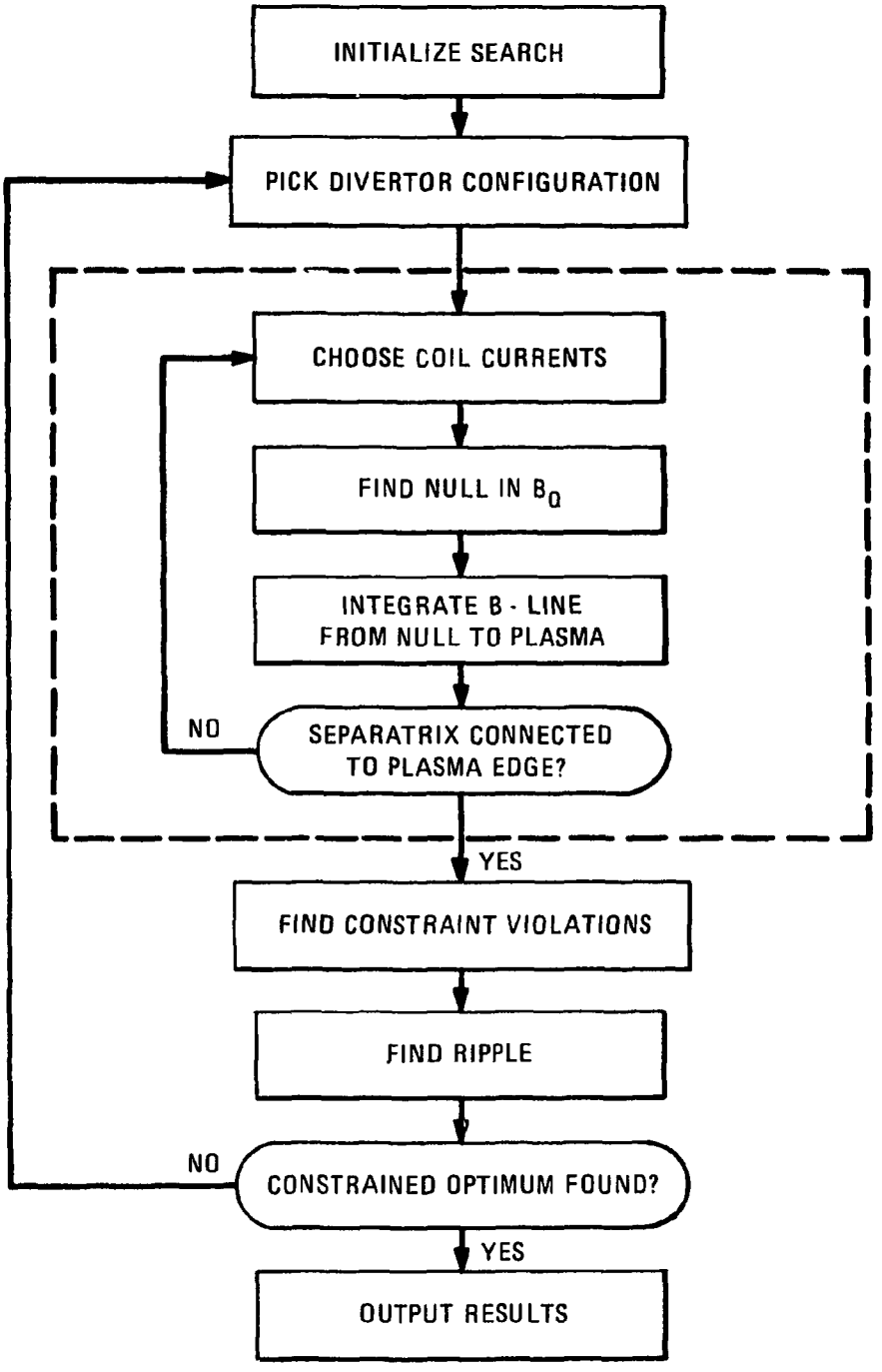

Fig. A.1